ICES REPORT 14-35

November 2014

History Matching of Production and Time-Lapse Seismic Data into Channelized Reservoir Models Using Ensemble Smoother

by

Reza Tavakoli, Sanjay Srinivasan, Ahmed H. ElSheikh, Mary F. Wheeler

The Institute for Computational Engineering and Sciences
The University of Texas at Austin
Austin, Texas 78712

Reference: Reza Tavakoli, Sanjay Srinivasan, Ahmed H. ElSheikh, Mary F. Wheeler, "History Matching of Production and Time-Lapse Seismic Data into Channelized Reservoir Models Using Ensemble Smoother," ICES REPORT 14-35, The Institute for Computational Engineering and Sciences, The University of Texas at Austin, November 2014.

History Matching of Production and Time-Lapse Seismic Data into Channelized Reservoir Models Using Ensemble Smoother

Reza Tavakoli[1], Sanjay Srinivasan[2], Ahmed H. ElSheikh[3], and Mary F. Wheeler[1]

[1]The Center for Subsurface Modeling (CSM), Institute for Computational Engineering and Sciences (ICES)[1]
[2]Department of Petroleum & Geosystems Engineering, University of Texas at Austin
[3]Institute of Petroleum Engineering, Heriot-Watt University, Edinburgh, UK

November 2014

[1]201 E. 24th Street, ACES 5.318, C0200, Austin, TX, 78712

Abstract

Ensemble-based algorithms have been successfully implemented for history matching of geological models. However, their performance is optimal only if the prior-state vector is linearly related to the predicted data and if the joint distribution of the prior-state vector is multivariate Gaussian. Moreover, the number of degrees of freedom is as large as the ensemble size, so the assimilation of large amounts of production or seismic data might lead to the ensemble collapse which results in inaccurate predictions of future performance. In this paper, we introduce a methodology that combines model classification with multidimensional scaling (MDS) and the ensemble smoother algorithm to efficiently history match fluvial and channelized reservoir models. The dynamic responses (production and seismic data) of the different ensemble members are used to compute a dissimilarity matrix. This dissimilarity matrix is then transformed into a lower-dimensional space by the use of MDS. Then, model classification is performed based on the distances between the mapped responses in the lower dimensional space and the actual observed response. In the proposed method, the transformed lower-dimensional data are used instead of original observations in the update equation to update the cluster of ensemble members that are closest to the observed response. In this manner, a limited number of ensemble members are enough to assimilate large amount of observed data without triggering the ensemble collapse problem. The updated subset of models (cluster) are used to infer a probability map and/or new hard conditioning data to re-sample new conditional members for the next iteration or next data-assimilation step. The proposed algorithm is tested by assimilating production and time-lapse seismic data into channelized reservoir models. The presented computational results show significant improvements in terms of preserving channelized features and in terms of reliability of predictions compared to the standard implementation of ensemble-based algorithms.

Contents

1 Introduction

Developing a complete description of model parameters involved in subsurface multi-phase flow models is a very challenging task as in many instances these parameters can not be measured directly. Direct measurements of reservoir properties are only available at a small number of well locations. The characterization of model parameters is often carried out by inferring useful information from a limited set of observations and combining that with geological interpretation in order to generate a geostatistical prior model. Frequently, the calibration of these model parameters is performed by minimizing the differences between the observed dynamic data and the corresponding model outputs. In reservoir engineering literature, the process of calibrating model parameters with nonlinear dynamic data is known as "history matching" [37]. Recent developments in reservoir history matching is presented in detail in a review paper by Oliver and Chen [36]. It is widely acknowledged that a single calibrated model cannot provide an accurate assessment of reservoir characteristics and the inherent uncertainty in representing those characteristics. The uncertainty stems from the fact that history matching is an ill-posed inverse problem with several non-unique solutions that match the measurements but produce different predictions.

Data assimilation is the process of continuously integrating observed data into dynamic models to determine the best estimate of uncertain parameters. The ensemble Kalman filter (EnKF) algorithm was introduced by Evensen [18, 19] for data assimilation in oceanographic and atmospheric models. Since its introduction, it has been used extensively in many applications including oceanography [5, 31], weather forecasting [28], hydrology [38, 8] and petroleum reservoir history matching [1, 36]. EnKF has been widely used mainly due to the ease of its implementation (sensitivity estimation is not required), its sequential updating scheme, and its computational efficiency. Alternatively, the ensemble smoother (ES) updates only the model parameters and assimilates all the measurements at once using a single analysis step [33]. By avoiding the frequent modification of simulator primary variables files (i.e., restart files), the ES performs much faster than the EnKF method. However, it has been shown that the EnKF outperforms the ES method with regard to accuracy [33, 22] because the overlapping effects of sequential updates keep the ensemble of states closer to the true solution. Iterative forms of ES have been proposed to improve its performance. Emerick and Reynolds [15] proposed a methodology for assimilating the same data multiple times (ES-MDA) with an inflated measurement error covariance matrix. They concluded that the ES-MDA resulted in better data matches than the EnKF with a comparable computational cost.

It is important to note that these ensemble-based algorithms are only optimal if the prior state vector is linearly related to the predicted data and if the joint distribution of the prior state vector is multivariate Gaussian [49]. These assumptions are certainly not true for multiphase flow problems and they can result in degraded performance of ensemble-based algorithms. Several authors have tried to develop techniques to improve the performance of ensemble-based algorithms for highly non-Gaussian problems that involved the modeling of facies and channelized reservoirs [34, 2, 50, 35, 7, 30, 42, 51, 11, 13].

A parameterization approach based on the truncated pluri-Gaussian model has been used for updating reservoir properties in models controlled by facies distributions by Liu and Oliver [34], Zhao et al [50]. They implemented the model for two-dimensional models and, subsequently, the method has been extended to three-dimensional reservoir models by Agbalaka and Oliver [2]. In this method, two or more Gaussian random fields are used to define reservoir regions corresponding to different facies, and then EnKF is used to update

the truncation surface used for modeling the spatial distribution of facies. Moreno and Aanonsen [35], and later Chang et al [7] combined a level set method with EnKF to preserve the continuty of facies boundaries during data assimilation. In their work, changes in facies boundaries were represented through level set functions. Other parameterization techniques such as discrete cosine transform (DCT) [30] and kernel principal component analysis (KPCA) [42] have also been used with EnKF during history matching of production data in multiple point statistics (MPS) reservoir models. Moreover, Jafarpour and Khodabakhshi [29] introduced a probability conditioning method (PCM) for conditioning facies simulation obtained using a given training image (TI) to nonlinear production data. They first obtained a probabilistic spatial map based on the ensemble of updated facies permeability values at the end of each EnKF update step and then used the resulting facies probability map to guide multiple point statistics (MPS) facies simulation. In a recent paper, ElSheikh et al [13] presented a Bayesian calibration method based on the nested sampling (NS) algorithm [43, 44, 12] for channelized models with MPS features. They introduced an efficient constrained sampling step into the NS algorithm based on obtaining a soft probability map of the channels locations. Moreover, the proposed algorithm provides an estimate of the Bayesian evidence for prior model selection. It is noted in all of the previous approaches, only the dynamic well production data is assimilated into the channelized reservoirs.

Although assimilation of well production data into reservoir models with ensemble-based algorithms has been frequently studied in the literature, the assimilation of time-lapse (4D) seismic data has gained interest in recent years and robust techniques for integrating that information are not well-established yet, especially for the channelized reservoir models. As the petro-physicists's interpretations of seismic data get more reliable, the utilization of time-lapse seismic data in reservoir characterization and management is increasing. The changes in the reservoir due to production and/or injection can be identified through interpretations of differences between a sequence of seismic surveys. Therefore, time-lapse seismic data could provide valuable information such as locations for infill drilling and mapping bypassed oil in the reservoir. Some applications of ensemble-based algorithms for assimilation of sesimic data has been already presented in the literature [10, 45, 23, 24, 16, 17]. However, there exist several challenges in assimilation of time-lapse seismic data into reservoir models. One of the challenges is to decide which kind of seismic data and at which level they can be integrated [25, 24]. Different types of time-lapse seismic data, such as amplitude difference data, shear and pressure waves impedance difference data, or pressure and saturation difference data, can be used for history matching (Figure 1). The information content and uncertainty of different types of data may vary a lot depending on the interpretation and inversion algorithms. Another significant challenge associated with assimilation of time-lapse seismic data is the large amount of available data. It is well known that for ensemble-based algorithms the number of degrees of freedom available to assimilate data is dictated by the size of the ensemble. Therefore, the limited size of an ensemble may not provide enough degrees of freedom to assimilate large amount of time-lapse seismic data. The variability of the ensemble may be reduced if the number of measurements exceeds the size of the ensemble and in the limit, after assimilating large amount of sesimic and/or production data, the ensemble collapses to a single realization. Moreover, this may cause spurious correlations between different components of state vector. The standard practice for reducing both the spurious correlations and the loss of variance is to use covariance localization [27, 3]. However, the adequate definition of a localization region, i.e. correlation lengths, is not trivial and requires additional considerations [14].

In a previous paper [48], we developed a methodology for production history matching of

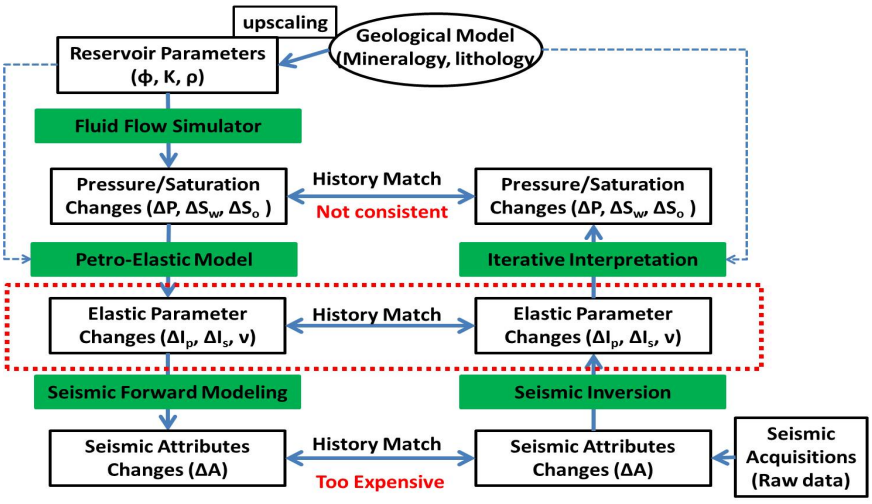

Figure 1: Different levels of time-lapse (4D) seismic data integration (modified from SPE 84464).

channelized reservoirs by combining model classification with MDS [41, 32, 6] and the EnKF. In this paper, we extend the application to integrate time-lapse seismic data. Although we use the ES algorithm in this paper, the proposed algorithm can also be used in conjunction with EnKF method. In the proposed algorithm, the responses (i.e. "modeled" production data and time-lapse seismic data) of the ensemble members are mapped to a lower dimensional space using MDS. Then, the models are clustered according to their distances from the actual observational data. The closest cluster to the actual observed response is updated using the ES equation. Moreover, the mapped seismic data (with low dimension) is used in the update equation. In this manner even a subset of ensemble is enough to assimilate large amount of seismic and/or production data without encountering ensemble collapse problem. The updated subset of models are then used to infer additional information from observation data. This additional information along with prior hard/soft data is used within a re-sampling procedure using a training image to enrich the selected ensemble for subsequent iterations of ES. The inferred information after the update step enforces the MPS features of the generated ensemble members.

This paper is organized as follows: In the next sections, we briefly present the methodology of ensemble-based algorithms such as EnKF, ES, and ES with multiple data assimilation (ES-MDA). This is followed with the detail descriptions of our proposed algorithm of combining MDS and ES. Then,the computational results and discussion are presented, followed by conclusions and a summary.

2 Methodology

2.1 Ensemble Kalman Filter.

In the EnKF implementations for history matching problems, we consider the vector of reservoir model parameters, such as grid block porosities and permeabilities, m, and the vector of primary state variables, p^n, such as grid block pressures and saturations, in an augmented state vector [21, 20], y^n:

$$y^n = \begin{bmatrix} m \\ p^n \end{bmatrix}, \tag{1}$$

where, the superscript n denotes the time at which we are assimilating data. The dimension of m is denoted as N_m and the dimension of p^n as N_p. Thus, the dimension of y^n, denoted by N_y is given as $N_y = N_m + N_p$. For simplicity of notation, we assume that the data is assimilated at every time step n to update N_e ensemble members. The predicted data for the jth ensemble member, $d_j^{n,f}$, can be obtained by running the reservoir simulator forward in time, which is represented by the nonlinear equation

$$d_j^{n,f} = g_n(m_j). \tag{2}$$

The predicted data, $d_j^{n,f}$, is a N_n-dimensional vector where N_n is the number of data points assimilated at the nth data assimilation time step. The EnKF update equation for each ensemble member j is given by

$$y_j^{n,a} = y_j^{n,f} + C_{YD}^{n,f}(C_{DD}^{n,f} + C_{D^n})^{-1}(d_{uc,j}^n - d_j^{n,f}) \quad \text{for } j = 1, 2, \cdots N_e. \tag{3}$$

Here, $C_{YD}^{n,f}$ is the $N_y \times N_n$ cross-covariance matrix between the forecast state vector and predicted data; $C_{DD}^{n,f}$ is the $N_n \times N_n$ auto-covariance matrix of predicted data; C_{D^n} is the $N_n \times N_n$ covariance matrix of observed data measurement errors; $d_{uc,j}^n$ is the vector of purturbed observations which is a sample from the normal distribution $\mathcal{N}(d_{\text{obs}}^n, C_{D^n})$ and d_{obs}^n represents the N_n-dimensional vector of observed data. The superscript f denotes the forecast or predicted data, the superscript a denotes the result of the assimilation step, and the subscript uc denotes an unconditional perturbation of observed data. The cross-covariance matrix, $C_{YD}^{n,f}$, and the auto-covariance matrix, $C_{DD}^{n,f}$, can be expressed by

$$C_{YD}^{n,f} = \frac{1}{N_e - 1} \sum_{j=1}^{N_e} \left(y_j^{n,f} - \bar{y}^{n,f}\right)\left(d_j^{n,f} - \bar{d}^{n,f}\right)^\top, \tag{4}$$

and

$$C_{DD}^{n,f} = \frac{1}{N_e - 1} \sum_{j=1}^{N_e} \left(d_j^{n,f} - \bar{d}^{n,f}\right)\left(d_j^{n,f} - \bar{d}^{n,f}\right)^\top, \tag{5}$$

where $\bar{y}^{n,f}$ and $\bar{d}^{n,f}$ denote the mean of the N_e predicted state vectors and the mean of the N_e predicted data at assimilation time-step n, respectively. The superscript $\top$ denotes the transpose of a matrix. Note in the implementation of the EnKF analysis Eq. (3) that the $N_y \times N_n$ matrix $C_{YD}^{n,f}$ as defined by (4) is never explicitly computed or stored.

2.2 Ensemble Smoother.

The ES method only updates model parameters m, instead of the full state vector y^n as in EnKF. Moreover, all the observation data are assimilated simultaneously. Therefore, the ES implementation could be considered as a parameter estimation algorithm that is consistent with traditional history matching problems. Thus, the updates for primary variables of simulator (such as pressure and saturation) are obtained by running reservoir simulation from time zero using the updated model parameters m. The ES update equation for each ensemble member is given by

$$m_j^a = m_j^f + C_{MD}^f (C_{DD}^f + C_D)^{-1}(d_{\mathrm{uc},j} - d_j^f) \qquad \text{for } j = 1, 2, \cdots N_e, \tag{6}$$

where C_{MD} is the $N_m \times N_d$ cross-covariance matrix between the prior vector of model parameters, m_j^f, and the N_d-dimensional vector of predicted data, d_j; C_{DD} is the $N_d \times N_d$ auto-covariance matrix of predicted data; $d_{\mathrm{uc},j}$ is the N_d-dimensional vector of perturbed observed data that contains total number of dynamic data for ensemble member j, i.e., $d_{\mathrm{uc},j} \sim \mathcal{N}(d_{\mathrm{obs}}, C_D)$ or equivalently

$$d_{\mathrm{uc},j} = d_{\mathrm{obs}} + C_D^{1/2} Z_j, \tag{7}$$

where d_{obs} is the N_d-dimensional vector of total number of measurments; C_D is the $N_d \times N_d$ covariance matrix of observed data measurement errors and Z_j is a normally distributed random vector, i.e. $Z_j \sim \mathcal{N}(0, I_{N_d})$. Note here for ES method, we let N_d denote the total number of measurements assimilated and since all the data are being assimilated simultaneously, we suppress the time superscript n in Eq. (6). The $N_m \times N_d$ cross-covariance matrix, C_{MD}^f, is defined as

$$C_{MD}^f = \frac{1}{N_e - 1} \sum_{j=1}^{N_e} \left(m_j^f - \bar{m}^f\right)\left(d_j^f - \bar{d}^f\right)^\top, \tag{8}$$

where $\bar{m}^f$ and $\bar{d}^f$ denote the mean of the prior model parameters and the predicted data, respectively. The auto-covariance matrix, C_{DD}^f, can be obtained using Eq. (5) without superscript n. Similar to the EnKF, the ES algorithm consists of two main steps, the forecast step and the analysis step. In the forecast step, each of the ensemble members is propagated in time from $t = 0$ to $t = t^N$, the time of last data assimilation. In the analysis step, the vector of predicted data, d_j, corresponding to all measured data, d_{obs}, is used in Eq. (6) to update the model parameters for each of the ensemble members.

2.3 Ensemble Smoother With Multiple Data Assimilation.

Although the implementation of the ES algorithm is much faster than the EnKF method, the results are not as satisfactory as those obtained with the EnKF. The performance of the ES and EnKF has been compared in an oceanography model by van Leeuwen and Evensen [33] and for a Lorenz model by Evensen and van Leeuwen [22]. In both cases, the EnKF performed better than the ES. van Leeuwen and Evensen [33] concluded that the relatively poor performance of the ensemble smoother compared to the EnKF is due to the poor prior estimate of uncertainty. In EnKF, the sequential updates "pull" the ensemble member toward the data at every assimilation time-step. Therefore, the posterior ensemble has a much lower variance. It is well known that the EnKF is similar to applying a single Gauss-Newton iteration at each data assimilation time-step with a full step size and average sensitivity matrix estimated from the ensemble [40, 26]. Motivated by this idea, Emerick and Reynolds [15] proposed a methodology to improve the performance of the ES with assimilating the same data multiple times (ES-MDA) with an inflated measurement error covariance matrix. In their procedure, Emerick and Reynolds [15] showed the equivalence between single and multiple data assimilation for linear models where the number of data assimilation, i.e. number of iterations, must be selected a priori in order to determine the inflation coefficients. This idea have also been discussed in an earlier work by Bergemann and Reich [4]. The update equation in the ES-MDA is similar to the update equation in

the ES (i.e. Eq. (6)), however, C_D is replaced by $\alpha_i C_D$, where the inflation coefficients, α_i, must be selected such that

$$\sum_{i=1}^{N_a} \frac{1}{\alpha_i} = 1, \tag{9}$$

where N_a denotes the number of data assimilation cycles or iterations.

3 Multidimensional Scaling with Ensemble Smoother.

In [48], we presented an algorithmic application of multidimensional scaling (MDS) with EnKF for history matching of channelized reservoirs. Multidimensional scaling (MDS) is a statistical technique that is often used to visualize high-dimensional data (N_d space) in an s-dimensional apace, where $s \ll N_d$. This is done by mapping high-dimensional data into a low-dimensional MDS space while retaining its original characteristics as much as possible [6]. In this section, we describe an efficient procedure for combining MDS and ES algorithms for assimilation of production and seismic data. We start the algorithm by rewritting the Eq. (6) of ES using Eq. (7) as follows

$$m_j^a = m_j^f + C_{MD}^f C_D^{-1/2} (C_D^{-1/2} C_{DD}^f C_D^{-1/2} + I_{N_d})^{-1} C_D^{-1/2} (d_{\text{obs}} + C_D^{1/2} Z_j - d_j^f) \qquad \text{for } j = 1, 2, \cdots N_e, \tag{10}$$

where $C_D^{-1/2}$ denotes the inverse of the square root of the covariance matrix C_D and I_{N_d} is the $N_d \times N_d$ identity matrix. We define the vector of scaled observation data and vector of scaled predicted data as $\tilde{d}_{\text{obs}} = C_D^{-1/2} d_{\text{obs}}$ and $\tilde{d}_j^f = C_D^{-1/2} d_j^f$, respectively. Then, it is straightforward to obtain

$$m_j^a = m_j^f + C_{M\tilde{D}}^f (C_{\tilde{D}\tilde{D}}^f + I_{N_d})^{-1} (\tilde{d}_{\text{obs}} + Z_j - \tilde{d}_j^f) \qquad \text{for } j = 1, 2, \cdots N_e, \tag{11}$$

where $C_{M\tilde{D}}$ is the $N_m \times N_d$ cross-covariance matrix between the prior vector of model parameters, m_j^f, and the N_d-dimensional vector of scaled predicted data, $\tilde{d}_j$, and $C_{\tilde{D}\tilde{D}}$ is the $N_d \times N_d$ auto-covariance matrix of scaled predicted data. The rest of the parameters have already been defined. Equation (11) suggests that the mapping into a lower dimensional space with MDS should be done based on scaled data. This is consistent with our previous implementations in [48] where the matrix of data was rescaled using the standard deviation of observed data measurement errors.

We now define the $N_d \times (N_e + 1)$ matrix D in N_d-dimensional space such that its first N_e columns hold the vector of scaled predicted data $\tilde{d}_j$ for all ensemble members and its $(N_e + 1)$th column holds the vector of scaled observation data $\tilde{d}_{\text{obs}}$:

$$D = \begin{bmatrix} \tilde{d}_1 & \tilde{d}_2 & \dots & \tilde{d}_{N_e} & \tilde{d}_{\text{obs}} \end{bmatrix}. \tag{12}$$

Similarly, we let $\hat{D}$ denote an $s \times (N_e + 1)$ matrix in s-dimensional space

$$\hat{D} = \begin{bmatrix} \hat{d}_1 & \hat{d}_2 & \dots & \hat{d}_{N_e} & \hat{d}_{\text{obs}} \end{bmatrix}. \tag{13}$$

where the s-dimensional vectors $\hat{d}_j$ correspond to the N_d-dimensional scaled data vectors $\tilde{d}_j$ for $j = 1, 2, ..., N_e + 1$ and $\hat{d}_{\text{obs}}$ denotes the vector of observation data in the s-dimensional space. The steps required to map the original N_d-dimensional data-space into

the s-dimensional space (with $s \ll N_d$) are detailed in [48]. After convergence of the MDS algorithm, we have N_e set of points (vectors) in the s-dimensional projected space, one for each of the ensemble members plus one additional point representing the projected observation data, i.e., $\hat{d}_{\text{obs}}$. The model responses in the projected space of reduced dimension (two- or three-dimension) can be visualized and plotted. Two models that are close to each other in this MDS (reduced dimension) space are indicative of similarity between the models. Conversely, models that are far apart from each other in the reduced space imply dissimilarity. Thus, the projected data can then be used to group models using a multivariate technique such as k-means clustering or kernel-PCA. Moreover, the projected vectors of predicted and observation data can be used in the ES update equation instead of the original data, i.e.,

$$m_j^a = m_j^f + C^f_{M\hat{D}}(C^f_{\hat{D}\hat{D}} + I_s)^{-1}(\hat{d}_{\text{obs}} + Z_j - \hat{d}_j^f) \qquad \text{for } j = 1, 2, \cdots N_c, \tag{14}$$

where $C_{M\hat{D}}$ is the $N_m \times s$ cross-covariance matrix between the prior vector of model parameters, m_j^f, and the s-dimensional vector of projected predicted data, $\hat{d}_j$; $C_{\hat{D}\hat{D}}$ is the $s \times s$ auto-covariance matrix of projected predicted data; I_s is the $s \times s$ identity matrix; and N_c denotes a subset of models (a cluster) that includes the observation point. Several observations can be made about the above algorithm:

1. One of the important benefit of rewriting ES update equation in the scaled form (Eq. (11)) is that after projecting data into s-dimensional space we do not need to devise a methodology to project measurement errors into the same space. The uncertainty in the data has been already incorporated in the MDS mapping by using scaled data. Hence, we do not have a $s \times s$ covariance matrix of projected observed data measurement errors, i.e. $C_{\hat{D}}$, in Eq. (11) and instead we only have the identity matrix I_s.

2. The ES implementation of Eq. (14) in the projected space has many advantages over the standard implementation of ES (i.e., Eqs. (6) or (11)) espacially when we assimilate large number of measurements like seismic data. First, the computational cost of inverting the $s \times s$ matrix $(C^f_{\hat{D}\hat{D}} + I_s)$ in Eq. (14) is much less than computing or inverting the $N_d \times N_d$ matrix $(C^f_{\tilde{D}\tilde{D}} + I_{N_d})$ in Eq. (11). Second, in the ensemble-based algorithms the number of degrees of freedom available to assimilate data is limited by the size of the ensemble. Thus, the ensemble may not provide enough degrees of freedom to assimilate original seismic data or large number of production data in the N_d-dimensional space. However, in the projected space where $s \ll N_d$, even small ensemble size is enough to assimilate large amount of seismic or/and production data without encountering ensemble collapse problem.

3. For visualization purposes we usually choose the subspace dimension s to be two or three dimensions. However, there is no restriction to pick any value less than N_d and thus the dataset can be mapped to any low-dimensional space, although it might be difficult to visualize the projection into any space greaqter than 3 dimensions.

4. In this paper, we implement ES using Eq. (14) to a subset of channelized models (N_c ensemble members) in order to retrieve new hard conditioning data or a probability map. Then a resampling procedure, as described in [48], is performed to obtain updated ensemble members. However, the proposed projected equation for ES algorithm, i.e. Eq. (14), is general, and it can be used to update model parameters of all N_e ensemble members for different history matching problems.

5. The computational cost of the proposed MDS algorithm is relatively small as the cost of mapping large amount of seismic and production data into a lower dimensional space is much less than of a single forward simulation run.

6. Although the focus of this paper is on the use ES method for fluvial and channelized reservoirs, the same procedure can be applied to obtain a similar equation as Eq. (14) for implementing EnKF method in the projected space.

Throughout, we refer to the above algorithm as MDS-ES algorithm. In summary, the first step is to utilize MDS to project the data (observed and predicted) of all the ensemble members into a lower-dimensional space. Then, we update the model parameters of a subset of selected members (N_c) using Eq. (11). In the next step, re-sampling [48] is performed to obtain an updated set of N_e ensemble members that share the common connectivity characteristics of the selected models. These updated ensemble members are the conditioned realizations after standard ES or after one step of the ES-MDA algorithm and are used as initial guess for the next ES-MDA iteration. The combined MDS and ES-MDA algorithms is referred to as MDS-ES-MDA algorithm.

4 Computational Example and Discussion

In this section, we evaluate the proposed algorithm using a two-dimensional, two-phase water flooding example. We first describe the problem setup, then we present the history matching results of the standard ES and ES-MDA algorithms. Then, we apply the proposed MDS-ES and MDS-ES-MDA algorithms to the same problem and compare the results with the standard ES implementation and discuss the benefits of the proposed algorithms. For all the experiments, we assimilate either only production data or both production and time lapse seismic data. In this paper, we use the commercial simulator IMEX 2013 [9] for flow stimulation. The parallel ensemble-based workflow as described in Tavakoli et al [47] has been used to conduct all the history matching experiments.

4.1 Example Description.

The reservoir model pertains to two-phase oil and water flow in a two-dimensional horizontal domain with 100×100 uniform Cartesian grid. The grid block sizes are $\Delta x = \Delta y =$ 50 ft and the reservoir thickness is uniform and is equal to 25 ft. The prior ensemble members and reference horizontal log-permeability field are generated using the single normal equation simulation (SNESIM) algorithm [46] within the software suite SGEMS [39]. The log-permeability ($ln(k)$) fields contain two different facies (shale and sand) and are drawn from a training image shown in Figure 2. The reference $ln(k)$ field and the location of wells are shown in Figure 3(a). The well configuration mimics four units of the five-spot pattern with four production wells and nine water injection wells. The production wells are constrained to a bottom hole pressure (BHP) of 3500 psi, and the injection wells are set to operate at a constant water injection rate of 1000 STB/day and maximum injection BHP of 6500 psi. The initial reservoir pressure and oil saturation are uniform and equal to 4000 psi and 0.8, respectively. The simulation starts at time zero, and all wells start operating at the beginning of the simulation. The measured production data are the oil and water rates (q_{oil} and q_{wat}) at production wells and BHP at injection wells. The data are recorded every 30 days for a period of 1020 days. The production observation data are generated by adding Gaussian noise to the simulation results with a noise level equal to 5% of the reference data.

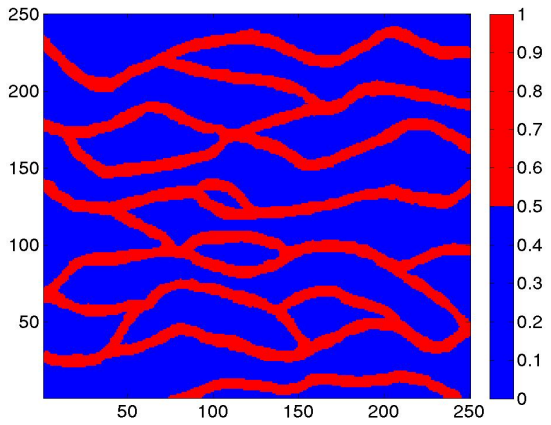

Figure 2: Training image used to generate reference field and realizations of log-permeability fields.

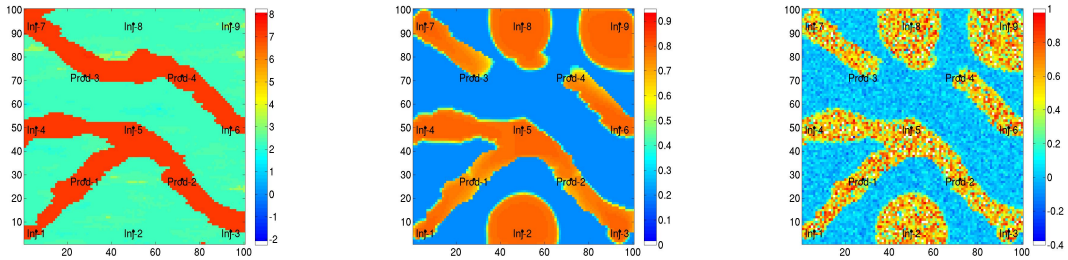

(a) (b) (c)

Figure 3: **(a)** Reference log-permeability field ($ln(k)$) with the location of wells identified. **(b)** Reference water saturation (S_w) distribution at 1020 days. **(c)** Seismic data (ΔS_w with noise) at 1020 days.

Here, we consider water saturation differences (ΔS_w) available throughout the grid. This might be the kind of information that might be extracted between a monitoring seismic survey at 1,020 days and a base survey at the initial conditions of the reservoir. The water saturation distribution is assumed to be known at the initial condition of the reservoir which is often not the case. These time-lapse saturation data are generated by adding correlated random noise to the simulated ΔS_w. We use an isotropic spherical covariance function, with standard deviation equal to 30% of grid blocks saturation changes and a range of 500 ft, to generate correlated random noise. The resulting time-lapse saturation changes are shown in Figure 3(c). The variance of the noise considered here is significant in order to mimic the errors and approximations associated with seismic inversion and the associated rock physics model. The production data for 1020 days and time-lapse saturation change data at 1020 days are assimilated in the reservoir models and, subsequently, the models are used to predict reservoir performance for an additional 1080 days. The uncertain model parameters are grid block log-permeabilities.

We performed data assimilation using standard ES, ES-MDA, MDS-ES, and MDS-ES-MDA algorithms with an ensemble size of $N_e = 100$ members. We conducted two sets of experiments: (1) assimilation of only production data. (2) assimilation of both production and saturation change data. The ES algorithm assimilates all observation data at the same

time in one step. To improve the results of the ES algorithm, we have performed multiple data assimilation steps by inflating the measurement error covariance matrix. In this work, we used the ES-MDA procedure as proposed by Emerick and Reynolds [15] with $N_a = 6$ and used the same data-covariance inflation factor in all the iterations, i.e., $\alpha_i = 6.0$ for $i = 1, 2, \cdots 6$. In the following sections, ESi denotes the i-th iteration of ES-MDA algorithm. For example, ES1 and ES6 correspond to the first and sixth iterations of ES-MDA, respectively.

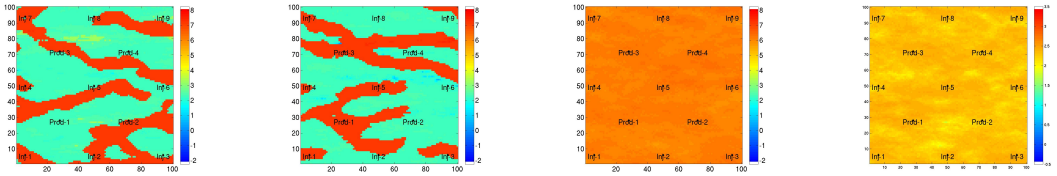

(a) (b) (c) (d)

Figure 4: Prior ensemble members, ensemble mean, and ensemble standard deviation of $ln(k)$. **(a)** and **(b)** Two randomly selected prior ensemble members. **(c)** prior ensemble mean. **(d)** prior standard deviation.

Figure 4 shows two randomly selected prior ensemble members, prior ensemble mean, and prior standard deviation of $ln(k)$ field. As can be seen from this figure, the prior ensemble mean (Figure 4(c)) is uniform, indicating that the channels are initially distributed randomly all over the domain among different ensemble members. The non-zero value of $ln(k)$ standard deviation (Figure 4(d)) also confirms the variabilities between individual prior realizations.

4.2 Standard ES and ES-MDA Results.

We now present results obtained with the standard ES and ES-MDA assimilating data six times (six iterations) with an ensemble size of $N_e = 100$ members. Figure 5 shows the final updated ensemble mean of $ln(k)$ fields after assimilation of only production data (first row) and both production and saturation change data (second row) using standard ES and ES-MDA algorithms. As can be seen from this figure, the standard implementations of ES and ES-MDA algorithms do not preserve the channels (facies) boundaries. The Gaussian assumption inherent in the ensemble-based algorithms transform the prior non-Gaussian $ln(k)$ distributions to a Gaussian distribution, and this causes the distinct differences between channel and non-channel facies to disappear. In other words, the multi-modal nature of $ln(k)$ of the reference field shown in Figure 6(a) can not be detected in the final ensemble mean obtained by ES-MDA as shown in Figure 6(b). It is also important to note from the results shown in the second row of Figure 5 that including the time-lapse seismic data in the assimilation processeven does not help in preserving the channel boundaries. The corresponding final standard deviation (STD) of $ln(k)$ after assimilation of production data and seismic data using standard ES and ES-MDA algorithms is shown in Figure 7. This figure shows that the assimilation of only production data using ES and ES-MDA reduces the STD of $ln(k)$ in the final ensemble members compared to the prior STD (Figure 4(d)). In general, the STD of $ln(k)$ decreases as a function of number of data assimilation cycles, i.e. iterations of ES-MDA, and increases as a function of distance from wells. However, the assimilation of both production data and time-lapse saturation/seismic data reduces the STD values of all the grid blocks to zero. In other word, there is no variability among different final ensemble members and the ensemble collapses to a single realization identical to the ensemble mean (Figure 5(e) or Figure 5(h)). As mentioned before the ensemble collapses is

attributed to the limited size of ensemble (here $N_e = 100$) which does not provide enough degrees of freedom to assimilate the large amount of production and seismic data (here N_d is more than 10,000).

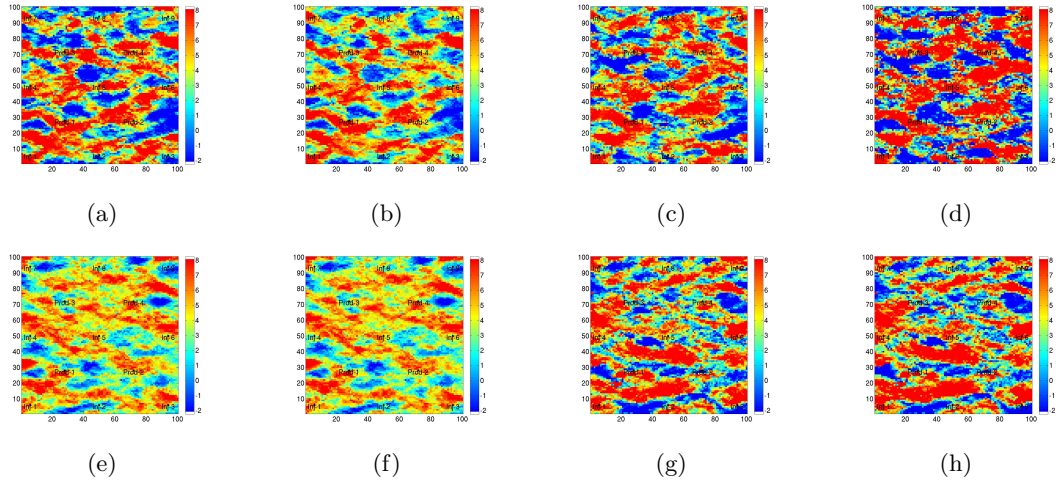

(a) (b) (c) (d)

(e) (f) (g) (h)

Figure 5: Final updated ensemble mean of $ln(k)$ after assimilation of only production data (first row) and both production and saturation change data (second row) using standard ES and ES-MDA algorithms. **(a)** and **(e)** standard ES. **(b)** and **(f)** ES1. **(c)** and **(g)** ES2. **(d)** and **(h)** ES6.

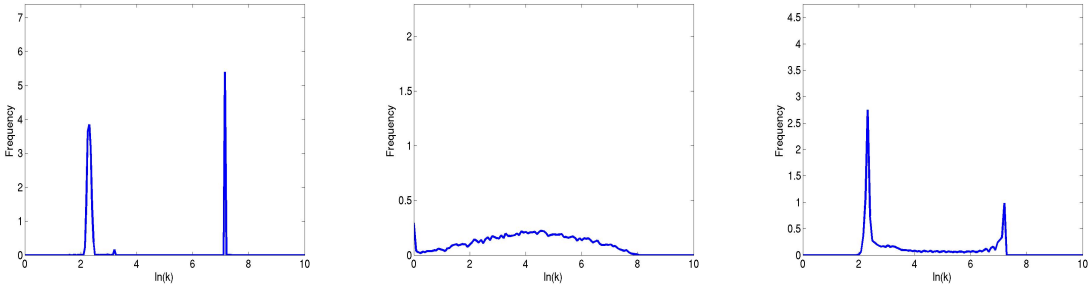

(a) (b) (c)

Figure 6: Histogram of $ln(k)$ fields for: **(a)** Reference model. **(b)** Final updated ensemble mean of $ln(k)$ obtained with standard ES-MDA (ES6). **(c)** Final updated ensemble mean of $ln(k)$ obtained with MDS-ES-MDA (ES6).

Figure 8 presents the history matching and production forecast of oil flow-rate (q_{oil}) of Prod-1. These results obtained by running simulation from time zero with the final ensemble members after assimilation of production data (first row) and both production and time-lapse seismic (saturation change) data (second row) with standard ES and ES-MDA algorithms. As can be seen from this figure, although assimilation of only production data with ES (Figure 8(a)) and ES-MDA (ES6, Figure 8(c)) reduces the initial large spread of q_{oil} of Prod-1, however, the final ensemble mean of prediction (green curve) does not provide good history match and prediction results. This poor history match result was also expected from the final ensemble mean of $ln(k)$ fields (Figures 5(a) and 5(d)) in which there was no features similarity with the reference model. The history matching results obtained with assimilation of both production and saturation change data (Figures 8(d) and 8(f)) show

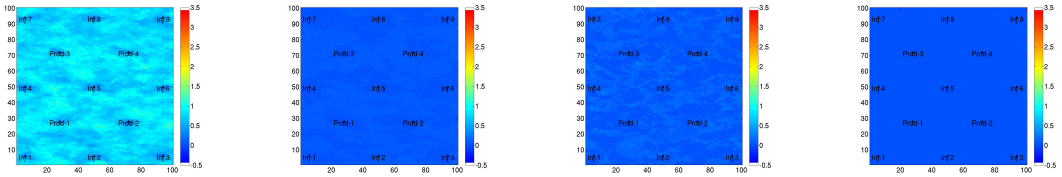

(a) (b) (c) (d)

Figure 7: Final standard deviation of $ln(k)$ after assimilation of production data and saturation change data using standard ES and ES-MDA algorithms. **(a)** standard ES with production data only. **(b)** standard ES with both production and saturation change data. **(c)** ES6 with production data only. **(d)** ES6 with both production and saturation change data.

that not only we have obtained poor history match and prediction results, but also the final (posterior) variability of ensemble members is reduced to a single point, especially for the case with multiple data assimilations (ES6). These results are consistent with the observed zero values of STD of $ln(k)$ from Figure 7(d). The history matching and prediction results of other wells and quantities (not shown here) are also of the same qualities as those shown in Figure 8.

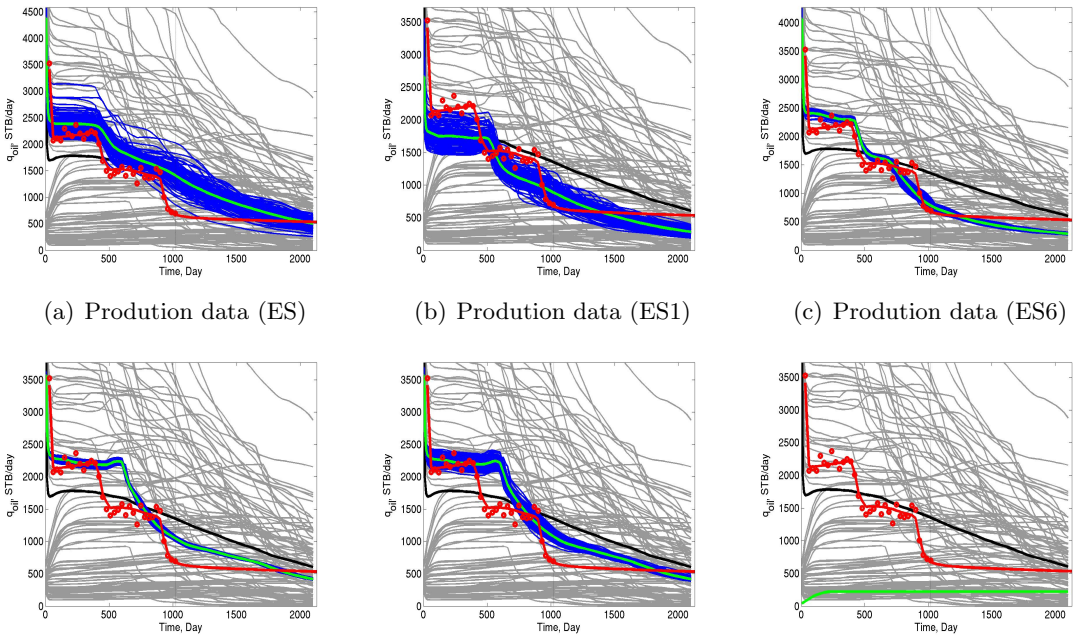

(a) Prodution data (ES) (b) Prodution data (ES1) (c) Prodution data (ES6)

(d) Prodution and Seismic (ES) (e) Prodution and Seismic (ES1) (f) Prodution and Seismic (ES6)

Figure 8: History matching and production forecasts of q_{oil} of Prod-1 from the final updated ensembles after assimilation of only production data (first row) and both production and saturation change data (second row) using standard ES and ES-MDA algorithms with $N_e = 100$. Open red circles are observed data, red curve is from the true model, green curve is the updated ensemble mean, blue curves represent updated ensemble predictions, gray curves represent prior ensemble predictions and black curve is the prior ensemble mean. The vertical line marks the end of historical data.

4.3 MDS-ES and MDS-ES-MDA Results.

We use MDS technique for two reasons: first, to isolate the ensemble members that produce prediction results as close as possible to the observation in the mapped space, and second, to reduce the large amount of assimilated–production and time-lapse seismic/saturation – data by mapping the data into a lower dimensional space. Moreover, the observed and predicted data can be visualized in two- or three-dimensional reduced space. Figure 9 shows the map of observation data (red dot) and ensemble responses (black and green dots) in three-dimensional MDS space for the first (ES1) and sixth (ES6) iterations of MDS-ES-MDA algorithm. It should be noted that the data here contains both production and saturation change data. As can be seen from this figure, the observed data point is far from the predicted data obtained with initial ensemble members (Figure 9(a)), whereas after multiple data assimilations the ensemble members are scattered around the observed data point (Figure 9(b)). In this section, we perfom clustering of ensemble members based on the distaces of predicted data from observed data and retain 30 ensemble members, i.e. $N_c = 30$. The selected cluster size is based on a sensitivity study (not shown here) similar to the one presented in Tavakoli et al [48]. In general, we approximately choose one third of prior realizations for the number of models within the selected cluster. It is important to notice that although we use a subset of ensemble members in the update equation, i.e. Eq. (14), we avoid encountering spurious correlations between components of the model parameters and predicted data vectors by operating on the mapped data instead of large vector of original data.

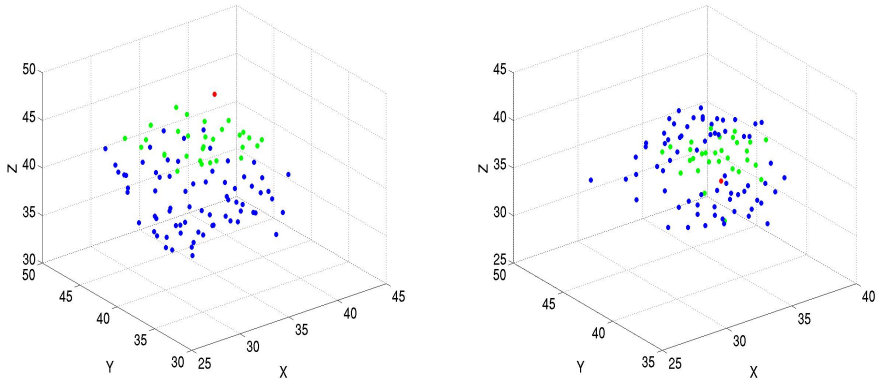

(a) (b)

Figure 9: Multidimensional Scaling (MDS) maps of reference (true) model and ensemble members response in 3D domain using MDS-ES-MDA algorithm. Red symbol is observation, blue symbols are ensemble members and green symbols are selected ensemble members. **(a)** ES1. **(b)** ES6.

Figure 10 presents the ensemble mean of $ln(k)$ fields obtained with the final ensemble after MDS-ES and MDS-ES-MDA. The results of this figure were obtained by assimilation of production data only (first row) and both production and saturation change data (second row). This figure shows clearly the improvement in preserving the channels boundaries compared to the results presented in Figure 5. As can be seen from this figure, the essential features of the reference model (Figure 3(a)) are captured in the final ensemble mean when using either MDS-ES or MDS-ES-MDA algorithms. This behaviour is largely due to the effect of resampling of additional ensemble members using the training image that share the

common characteristics observed in the selected cluster. Moreover, the resampled realizations follow the non-Gaussian (multi-modal) distribution. As can be seen from Figure 6(c), the histogram of final ensemble mean of $ln(k)$ obtained after the last iteration of MDS-ES-MDA (ES6) shows multi-modal distribution similar to those present in the reference model (Figure 6(a)). Comparing the first and the second rows of Figure 10, we observe that the assimilation of both production and saturation change data data improves the final history matched ensemble mean of $ln(k)$. In particular, the spurious channels that exist in the final ensemble mean of $ln(k)$ obtained with assimilation of only production data (highlighted with oval in the first row of Figure 10) are eliminated or diminished when we assimilate simultaneously both the production and seismic data simultaneously.

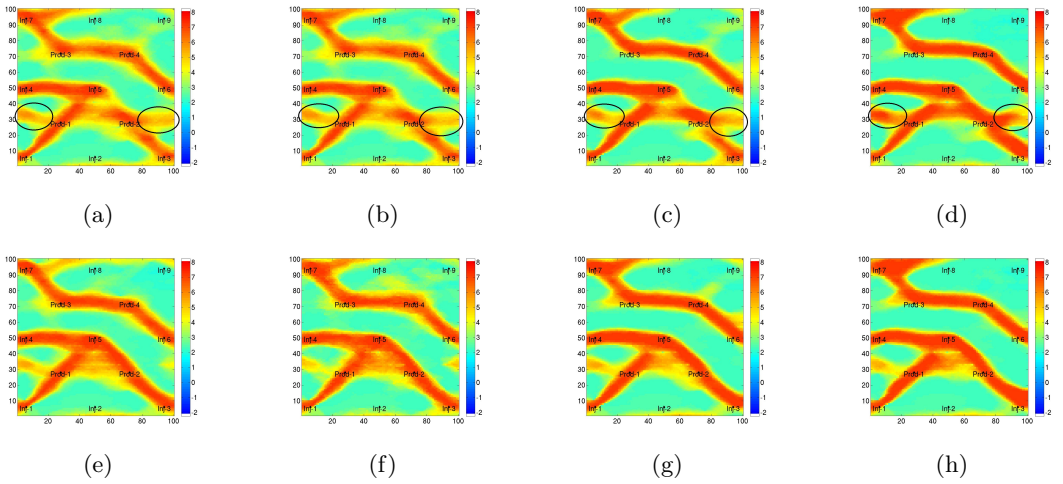

(a) (b) (c) (d)

(e) (f) (g) (h)

Figure 10: Final updated ensemble mean of $ln(k)$ after assimilation of only production data (first row) and both production and saturation change data (second row) using MDS-ES and MDS-ES-MDA algorithms. **(a)** and **(e)** standard ES. **(b)** and **(f)** ES1. **(c)** and **(g)** ES2. **(d)** and **(h)** ES6.

Figure 11 presents the STD of $ln(k)$ after production and saturation data assimilation using MDS-ES and MDS-ES-MDA algorithms. According to results shown in this figure, we observe a significant reduction in STD compared to the prior STD presented in the Figure 4(d). Moreover, most of the remaining variabilities are at the boundaries of the existing channels. The results of final ensemble mean of $ln(k)$ in Figure 10 together with non-zero final STD of $ln(k)$ in Figure 11 confirm the importance of assimilation of large amount of data. The non-zero values of STD indicates the success of the proposed algorithm in mitigating the problem of ensemble collapse to a single deterministic solution.

Figure 12 presents the oil production flow-rate of Prod-1 obtained by running simulation from time zero with the final ensemble members after assimilation of production data (first row) and both production and seismic/saturation change data (second row) with MDS-ES and MDS-ES-MDA algorithms. Consistent with the improved reproduction of channelized features in the final permeability fields (Figure 10), the history matching results are also of high quality. As can be seen from this figure, the posterior ensemble spread (blue curves) is narrower than the prior ensemble spread (gray curves) and at the same time the posterior mean (green curve) follows the reference result during both the history match and prediction phases. In comparison to the history matching results shown in Figures 8(d) and 8(f), the posterior ensemble members do not collapse to a single realization when we assimilate both production and saturation change data using MDS-ES and MDS-ES-MDA. The non-zero

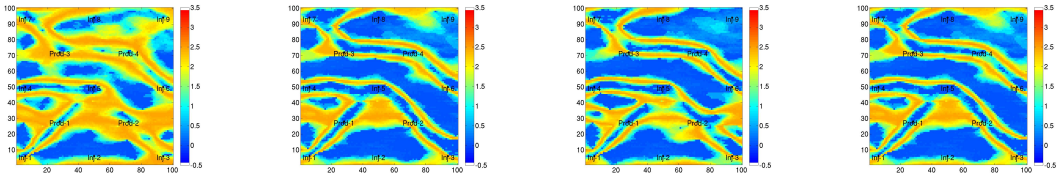

(a) (b) (c) (d)

Figure 11: Final standard deviation of $ln(k)$ after assimilation of production data and saturation change data using MDS-ES and MDS-ES-MDA algorithms. **(a)** MDS-ES with production data only. **(b)** MDS-ES with both production and saturation change data. **(c)** ES6 with production data only. **(d)** ES6 with both production and saturation change data.

posterior spread of the production prediction from the final ensemble members after assimilation of saturation change data is not surprising considering the non-zero values of STD of $ln(k)$ shown in Figures 11(b) and 11(d). It is important to mention that the resampling of models using the training image after data assimilation introduces models that exhibit some variation in the dynamic characteristics. these weakly constrained reservoir models reproduce production data that falls within the tails of the posterior distribution as shown in results of q_{oil} of Prod-1. The prediction results of other wells (not shown) exhibit similar quantitative results to those shown in Figure 12.

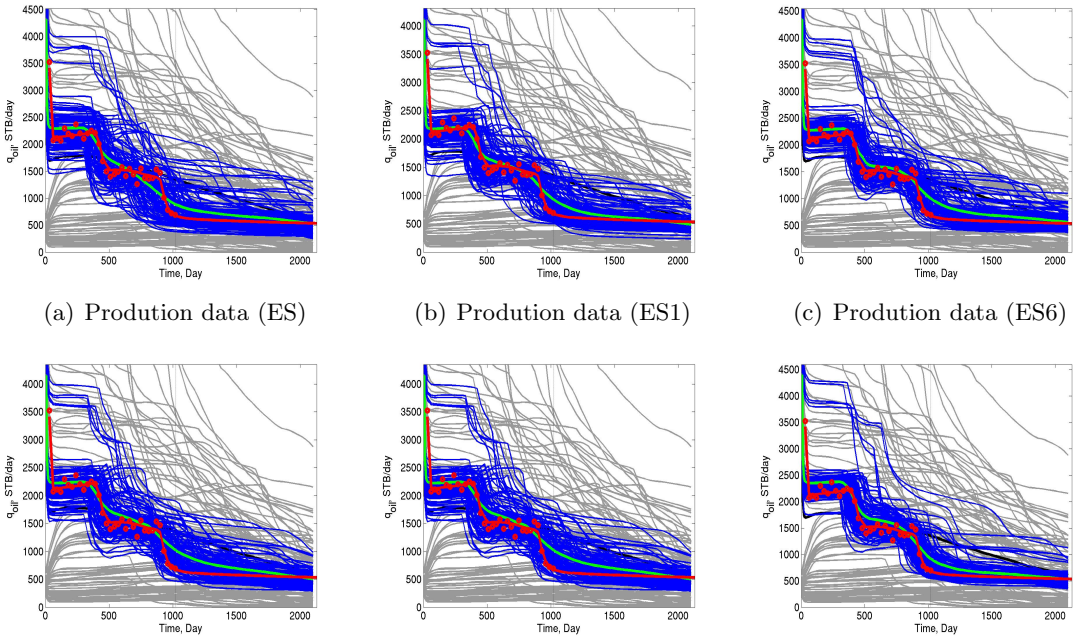

(a) Prodution data (ES) (b) Prodution data (ES1) (c) Prodution data (ES6)

(d) Prodution and Seismic (ES) (e) Prodution and Seismic (ES1) (f) Prodution and Seismic (ES6)

Figure 12: History matching and production forecasts of q_{oil} of Prod-1 from the final updated ensembles after assimilation of only production data (first row) and both production and saturation change data (second row) using MDS-ES and MDS-ES-MDA algorithms with $N_e = 100$. The curves in this figure have the same meaning as in Figure 8.

5 Summary and Conclusions

We have developed a new algorithm for history matching of fluvial and channelized reservoir based on combining multidimensional scaling (MDS) with the ensemble smoother (ES) method, namely MDS-ES. The importance of MDS, used in this work, is two-fold, first, to select the ensemble members with dynamic responses closest to the measured values. This subset of ensemble members is enriched by the information inferred from the measurements and used to improve the characteristics of the final ensemble after data assimilation. Second, to use lower dimensional (mapped) data in the update step of the ensemble-based algorithms. This is motivated by the limited number of degrees of freedom available to assimilate data which is dictated by the ensemble size. Trying to assimilate large amounts of production and seismic data without the application of MDS might results in the ensemble collapse to a single realizations with zero variability. However, in the projected space, where the data dimension is much lower than the size of original data (N_d), even a subset of ensemble is enough to assimilate large amount of seismic and/or production data without encountering ensemble collapse problem. Another important feature of MDS is that the observed data and prediction results can be visulaized in lower-order two- or three-dimensional space. Model clustering can be performed in this lower-dimensional space.

In the proposed algorithm we combined MDS with ES-MDA in which data are assimilated multiple times to improve the history matching results. In the standard implementations of ES-MDA, multiple data assimilations (iterations) destroy the channel boundaries and smear the distinct differences between channel and non-channel facies. Whereas in the combined MDS-ES-MDA, the resampling from training image with the "enriched" input data, after each step o data assimilation, improves the characterizations of the final ensemble by preserving the multi-modal features.

The developed algorithms have been applied to a fluvial reservoir model where both production and time-lapse seismic data have been assimilated. The standard ES and ES-MDA obtained very poor final ensemble of log-permeability fields compared to the reference model in both cases of assimilation of production data only and assimilation of both production and seismic data. Moreover, the final history matched models and corresponding predictions were not reasonable. Moreover, including time-lapse seismic data caused the ensemble to collapse to a single realization far from the reference model. However, the developed MDS-ES and MDS-ES-MDA yielded better results in terms of: (1) preserving the channel features and characteristics in the final ensemble, (2) obtaining reasonable history match and production forecast, and (3) reduction of large prior uncertainties in the model parameters and maintaining some variabilities between the different posterior ensemble members. It is also important to mention that for the example considered in this paper, saturation change data helped to improve the characteristics of the final ensemble mean of log-permeability. As such the predictions of future reservoir performance are expected to be more accurate using the updated models obtained with assimilation of both production and seismic data.

6 Nomenclature

C_D	=	covariance matrix of measurement errors
C_{DD}	=	auto-covariance matrix for predicted data
C_{MD}	=	cross-covariance between model parameters and predicted data
C_{YD}	=	cross-covariance between state vactor and predicted data
d	=	data vector
D	=	matrix of data
$g(.)$	=	forward model
I	=	identity matrix
$ln(k)$	=	log-permeability
s	=	reduced space dimension
m	=	vector of model parameters
N_c	=	number of chosen ensemble members
N_d	=	number of data
N_e	=	number of ensemble members
N_m	=	number of model parameters
N_p	=	number of dynamic parameters
p	=	vector of dynamic parameters
y	=	vector of state variables
Y	=	matrix of ensemble members
Z	=	vector of normal random deviate
α	=	inflation coefficient
ΔS_w	=	change of water saturation

7 Subscripts

BHP	=	bottom hole pressure
j	=	ensemble member index
obs	=	observed
uc	=	unconditional realization

8 Superscripts

a	=	analysis
f	=	forecast
n	=	time index
$^\top$	=	transpose
-1	=	inverse

9 Acknowledgments

A portion of this research was supported by the U.S. Department of Energy, Office of Science, Office of Basic Energy Sciences. The Center for Frontiers of Subsurface Energy Security (CFSES) is a DOE Energy Frontier Research Center, under Contract No. DE-SC0001114. The National Science Foundation (NSF) funding is also very gratefully appreciated.

Bibliography

[1] Aanonsen SI, Nævdal G, Oliver DS, Reynolds AC, Vallès B (2009) The ensemble Kalman filter in reservoir engineering–a Review. SPE Journal 14(3):393–412, DOI 10.2118/117274-PA

[2] Agbalaka C, Oliver DS (2008) Application of the EnKF and localization to automatic history matching of facies distribution and production data. Mathematical Geosciences 40

[3] Anderson JL (2007) Exploring the need for localization in ensemble data assimilation using a hierarchical ensemble filter. Physica D: Nonlinear Phenomena 230(1–2):99–111

[4] Bergemann K, Reich S (2010) A mollified ensemble Kalman filter. Quarterly Journal of the Royal Meteorological Society 136(651):1636–1643

[5] Bertino L, Evensen G, Wackernagel H (2003) Sequential data assimilation techniques in oceanography. International Statistical Review 71(2):223–241

[6] Borg I, Groenen P (1997) Modern multidimensional scaling: theory and applications. Springer, New York

[7] Chang H, Zhang D, Lu Z (2010) History matching of facies distribution with the enkf and level set parameterization. Journal of Computational Physics 229(20):8011–8030

[8] Chen Y, Zhang D (2006) Data assimilation for transient flow in geologic formations via ensemble Kalman filter. Advances in Water Resources 29(8):1107–1122

[9] CMG (2013) "IMEX User's Guide," Computer Modeling Group, Homepage: http://www.cmgl.ca/. Calgary, Alberta, Canada

[10] Dong Y, Gu Y, Oliver DS (2006) Sequential assimilation of 4D seismic data for reservoir description using the ensemble Kalman filter. Journal of Petroleum Science and Engineering 53(1–2):83–99

[11] Dovera L, Rossa ED (2011) Multimodal ensemble kalman filtering using gaussian mixture models. Computational Geosciences 15(2):307–323

[12] ElSheikh AH, Wheeler WF, Hoteit I (2013) Nested sampling algorithm for subsurface flow model selection, uncertainty quantification, and nonlinear calibration. Water Resources Research 49(12):8383–8399

[13] ElSheikh AH, Demyanov V, Tavakoli R, Christie MA, Wheeler MF (2014) Calibration of channelized subsurface flow models using nested sampling and soft probabilities. Advances in Water Resources p 33, DOI 10.1016/j.advwatres.2014.10.006

[14] Emerick A, Reynolds A (2010) Combining sensitivities and prior information for covariance localization in the ensemble kalman filter for petroleum reservoir applications. Computational Geosciences 15(2):251–269

[15] Emerick A, Reynolds A (2012) Ensemble smoother with multiple data assimilation. Computers & Geosciences DOI http://dx.doi.org/10.1016/j.cageo.2012.03.011

[16] Emerick A, Reynolds A (2012) History matching time-lapse seismic data using the ensemble kalman filter with multiple data assimilations. Computational Geosciences 16(3):639–659

[17] Emerick AA (2014) Estimation of pressure and saturation fields from time-lapse impedance data using the ensemble smoother. Journal of Geophysics and Engineering 11(3):035,007

[18] Evensen G (1994) Sequential data assimilation with a nonlinear quasi-geostrophic model using Monte Carlo methods to forecast error statistics. Journal of Geophysical Research 99(C5):10,143–10,162

[19] Evensen G (2005) The combined parameter and state problem. In: Technical Report, Norsk Hydro Research Center

[20] Evensen G (2007) Data Assimilation: The Ensemble Kalman Filter. Springer

[21] Evensen G (2009) The ensemble kalman filter for combined state and parameter estimation. IEEE Control Systems Magazine 29(3):83–104

[22] Evensen G, van Leeuwen PJ (2000) An ensemble Kalman smoother for nonlinear dynamics. Monthly Weather Review 128(6):1852–1867

[23] Fahimuddin A, Aanonsen SI, Skjervheim JA (2010) 4d seismic history matching of a real field case with enkf: use of local analysis for model updating. In: Proceedings of the SPE Annual Technical Conference and Exhibition. Florence, Italy, pp 19–22

[24] Fahimuddin A, Aanonsen SI, Skjervheim JA (2010) Ensemble based 4d seismic history matching–integration of different levels and types of seismic data (spe-131453). In: 72nd EAGE Conference & Exhibition

[25] Gosselin O, Aanonsen SI, Aavatsmark I, Cominelli A, Gonard R, Kolasinski M, Ferdinandi F, Kovacic L, Neylon K (2004) History matching using time-lapse seismic (HUTS). Journal of petroleum technology 56(4):66–67

[26] Gu Y, Oliver DS (2007) An iterative ensemble Kalman filter for multiphase fluid flow data assimilation. SPE Journal 12(4):438–446

[27] Houtekamer PL, Mitchell HL (2001) A sequential ensemble Kalman filter for atmospheric data assimilation. Monthly Weather Review 129(1):123–137

[28] Houtekamer PL, Mitchell HL, Pellerin G, Buehner M, Charron M, Spacek L, Hansen B (2005) Atmospheric data assimilation with an ensemble Kalman filter: Results with real observations. Monthly Weather Review 133(3):604–620

[29] Jafarpour B, Khodabakhshi M (2011) A probability conditioning method (pcm) for nonlinear flow data integration into multiple-point statistical facies simulation. Math Geosci 43(2):133–164, DOI 10.1007/s11004-011-9316-y

[30] Jafarpour B, McLaughlin DB (2009) Estimating channelized reservoir permeabilities with the ensemble Kalman filter: The importance of ensemble design. SPE Journal 14(2):374–388

[31] Keppenne CL (2000) Data assimilation into a primitive-equation model with a parallel ensemble Kalman filter. Monthly Weather Review 128(6):1971–1981

[32] Kruskal J, Wish M (1978) Multidimensional Scaling. Sage University Paper series on Quantitative Applications in the Social Sciences (07–011)

[33] van Leeuwen PJ, Evensen G (1996) Data assimilation and inverse methods in terms of a probabilistic formulation. Monthly Weather Review 124:2898–2913

[34] Liu N, Oliver DS (2005) Ensemble Kalman filter for automatic history matching of geologic facies. Journal of Petroleum Science and Engineering 47(3–4):147–161

[35] Moreno D, Aanonsen SI (2007) Stochastic facies modelling using the level set method. In: Extended abstracts book of Petroleum Geostatistics 2007, Cascais, Portugal, A18

[36] Oliver DS, Chen Y (2010) Recent progress on reservoir history matching: a review. Computational Geosciences 15(1):185–221

[37] Oliver DS, Reynolds AC, Liu N (2008) Inverse Theory for Petroleum Reservoir Characterization and History Matching. Cambridge University Press, Cambridge, UK

[38] Reichle RH, McLaughlin DB, Entekhabi D (2002) Hydrologic data assimilation with the ensemble Kalman filter. Monthly Weather Review 130(1):103–114

[39] Remy N, Boucher A, Wu J (2009) Applied Geostatistics with SGeMS : A User's Guide. ISBN: 9780521514149, Cambridge University Press

[40] Reynolds AC, Zafari M, Li G (2006) Iterative forms of the ensemble Kalman filter. In: 10th European Conference on the Mathematics of Oil Recovery, Amsterdam, the Netherlands, a030

[41] Romney AK, Shepard RN, Nerlove SB (1972) Multidimensional Scaling, Theory and Applications in the Behavioral Sciences. New York: Seminar Press 2 vols

[42] Sarma P, Chen WH (2009) Generalization of the ensemble Kalman filter using kernels for non-gaussian random fields. SPE 119177, presented at the SPE Reservoir Simulation Symposium, February 2-4, 2009

[43] Skilling J (2004) Nested sampling. Bayesian inference and maximum entropy methods in science and engineering 735:395–405

[44] Skilling J (2006) Nested sampling for general bayesian computation. Bayesian Analysis 1(4):833–859

[45] Skjervheim JA, Evensen G, Aanonsen SI, Ruud BO, Johansen TA (2007) Incorporating 4D seismic data in reservoir simulation models using ensemble Kalman filter. SPE Journal 12(3):282–292, DOI 10.2118/95789-PA

[46] Strebelle S (2002) Conditional simulation of complex geological structures using multiple-point statistics. Mathematical Geology 34(1):1–22

[47] Tavakoli R, Pencheva G, Wheeler MF, Ganis B (2012) A parallel ensemble-based framework for reservoir history matching and uncertainty characterization. Computational Geosciences 17(1):83–97, DOI 10.1007/s10596-012-9315-1

[48] Tavakoli R, Srinivasan S, Wheeler MF (2014) Rapid updating of utochastic models using an ensemble filter approach. SPE Journal 19(3):500–513, DOI http://dx.doi.org/10.2118/163673-PA

[49] Zafari M, Reynolds AC (2007) Assessing the uncertainty in reservoir description and performance predictions with the ensemble Kalman filter. SPE Journal 12(3):382–391, SPE 95750-PA

[50] Zhao Y, Reynolds AC, Li G (2008) Generating facies maps by assimilating production data and seismic data with the ensemble Kalman filter(SPE-113990). In: 2008 SPE Improved Oil Recovery Symposium

[51] Zhou H, Gomez-Hernandez J, Franssen HJH, Li L (2011) An approach to handling non-gaussianity of parameters and state variables in ensemble kalman filtering. Advances in Water Resources 34:844–864

Bibliography

[1] Aanonsen SI, Nævdal G, Oliver DS, Reynolds AC, Vallès B (2009) The ensemble Kalman filter in reservoir engineering–a Review. SPE Journal 14(3):393–412, DOI 10.2118/117274-PA

[2] Agbalaka C, Oliver DS (2008) Application of the EnKF and localization to automatic history matching of facies distribution and production data. Mathematical Geosciences 40

[3] Anderson JL (2007) Exploring the need for localization in ensemble data assimilation using a hierarchical ensemble filter. Physica D: Nonlinear Phenomena 230(1–2):99–111

[4] Bergemann K, Reich S (2010) A mollified ensemble Kalman filter. Quarterly Journal of the Royal Meteorological Society 136(651):1636–1643

[5] Bertino L, Evensen G, Wackernagel H (2003) Sequential data assimilation techniques in oceanography. International Statistical Review 71(2):223–241

[6] Borg I, Groenen P (1997) Modern multidimensional scaling: theory and applications. Springer, New York

[7] Chang H, Zhang D, Lu Z (2010) History matching of facies distribution with the enkf and level set parameterization. Journal of Computational Physics 229(20):8011–8030

[8] Chen Y, Zhang D (2006) Data assimilation for transient flow in geologic formations via ensemble Kalman filter. Advances in Water Resources 29(8):1107–1122

[9] CMG (2013) "IMEX User's Guide," Computer Modeling Group, Homepage: http://www.cmgl.ca/. Calgary, Alberta, Canada

[10] Dong Y, Gu Y, Oliver DS (2006) Sequential assimilation of 4D seismic data for reservoir description using the ensemble Kalman filter. Journal of Petroleum Science and Engineering 53(1–2):83–99

[11] Dovera L, Rossa ED (2011) Multimodal ensemble kalman filtering using gaussian mixture models. Computational Geosciences 15(2):307–323

[12] ElSheikh AH, Wheeler WF, Hoteit I (2013) Nested sampling algorithm for subsurface flow model selection, uncertainty quantification, and nonlinear calibration. Water Resources Research 49(12):8383–8399

[13] ElSheikh AH, Demyanov V, Tavakoli R, Christie MA, Wheeler MF (2014) Calibration of channelized subsurface flow models using nested sampling and soft probabilities. Advances in Water Resources p 33, DOI 10.1016/j.advwatres.2014.10.006

[14] Emerick A, Reynolds A (2010) Combining sensitivities and prior information for covariance localization in the ensemble kalman filter for petroleum reservoir applications. Computational Geosciences 15(2):251–269

[15] Emerick A, Reynolds A (2012) Ensemble smoother with multiple data assimilation. Computers & Geosciences DOI http://dx.doi.org/10.1016/j.cageo.2012.03.011

[16] Emerick A, Reynolds A (2012) History matching time-lapse seismic data using the ensemble kalman filter with multiple data assimilations. Computational Geosciences 16(3):639–659

[17] Emerick AA (2014) Estimation of pressure and saturation fields from time-lapse impedance data using the ensemble smoother. Journal of Geophysics and Engineering 11(3):035,007

[18] Evensen G (1994) Sequential data assimilation with a nonlinear quasi-geostrophic model using Monte Carlo methods to forecast error statistics. Journal of Geophysical Research 99(C5):10,143–10,162

[19] Evensen G (2005) The combined parameter and state problem. In: Technical Report, Norsk Hydro Research Center

[20] Evensen G (2007) Data Assimilation: The Ensemble Kalman Filter. Springer

[21] Evensen G (2009) The ensemble kalman filter for combined state and parameter estimation. IEEE Control Systems Magazine 29(3):83–104

[22] Evensen G, van Leeuwen PJ (2000) An ensemble Kalman smoother for nonlinear dynamics. Monthly Weather Review 128(6):1852–1867

[23] Fahimuddin A, Aanonsen SI, Skjervheim JA (2010) 4d seismic history matching of a real field case with enkf: use of local analysis for model updating. In: Proceedings of the SPE Annual Technical Conference and Exhibition. Florence, Italy, pp 19–22

[24] Fahimuddin A, Aanonsen SI, Skjervheim JA (2010) Ensemble based 4d seismic history matching–integration of different levels and types of seismic data (spe-131453). In: 72nd EAGE Conference & Exhibition

[25] Gosselin O, Aanonsen SI, Aavatsmark I, Cominelli A, Gonard R, Kolasinski M, Ferdinandi F, Kovacic L, Neylon K (2004) History matching using time-lapse seismic (HUTS). Journal of petroleum technology 56(4):66–67

[26] Gu Y, Oliver DS (2007) An iterative ensemble Kalman filter for multiphase fluid flow data assimilation. SPE Journal 12(4):438–446

[27] Houtekamer PL, Mitchell HL (2001) A sequential ensemble Kalman filter for atmospheric data assimilation. Monthly Weather Review 129(1):123–137

[28] Houtekamer PL, Mitchell HL, Pellerin G, Buehner M, Charron M, Spacek L, Hansen B (2005) Atmospheric data assimilation with an ensemble Kalman filter: Results with real observations. Monthly Weather Review 133(3):604–620

[29] Jafarpour B, Khodabakhshi M (2011) A probability conditioning method (pcm) for nonlinear flow data integration into multiple-point statistical facies simulation. Math Geosci 43(2):133–164, DOI 10.1007/s11004-011-9316-y

[30] Jafarpour B, McLaughlin DB (2009) Estimating channelized reservoir permeabilities with the ensemble Kalman filter: The importance of ensemble design. SPE Journal 14(2):374–388

[31] Keppenne CL (2000) Data assimilation into a primitive-equation model with a parallel ensemble Kalman filter. Monthly Weather Review 128(6):1971–1981

[32] Kruskal J, Wish M (1978) Multidimensional Scaling. Sage University Paper series on Quantitative Applications in the Social Sciences (07–011)

[33] van Leeuwen PJ, Evensen G (1996) Data assimilation and inverse methods in terms of a probabilistic formulation. Monthly Weather Review 124:2898–2913

[34] Liu N, Oliver DS (2005) Ensemble Kalman filter for automatic history matching of geologic facies. Journal of Petroleum Science and Engineering 47(3–4):147–161

[35] Moreno D, Aanonsen SI (2007) Stochastic facies modelling using the level set method. In: Extended abstracts book of Petroleum Geostatistics 2007, Cascais, Portugal, A18

[36] Oliver DS, Chen Y (2010) Recent progress on reservoir history matching: a review. Computational Geosciences 15(1):185–221

[37] Oliver DS, Reynolds AC, Liu N (2008) Inverse Theory for Petroleum Reservoir Characterization and History Matching. Cambridge University Press, Cambridge, UK

[38] Reichle RH, McLaughlin DB, Entekhabi D (2002) Hydrologic data assimilation with the ensemble Kalman filter. Monthly Weather Review 130(1):103–114

[39] Remy N, Boucher A, Wu J (2009) Applied Geostatistics with SGeMS : A User's Guide. ISBN: 9780521514149, Cambridge University Press

[40] Reynolds AC, Zafari M, Li G (2006) Iterative forms of the ensemble Kalman filter. In: 10th European Conference on the Mathematics of Oil Recovery, Amsterdam, the Netherlands, a030

[41] Romney AK, Shepard RN, Nerlove SB (1972) Multidimensional Scaling, Theory and Applications in the Behavioral Sciences. New York: Seminar Press 2 vols

[42] Sarma P, Chen WH (2009) Generalization of the ensemble Kalman filter using kernels for non-gaussian random fields. SPE 119177, presented at the SPE Reservoir Simulation Symposium, February 2-4, 2009

[43] Skilling J (2004) Nested sampling. Bayesian inference and maximum entropy methods in science and engineering 735:395–405

[44] Skilling J (2006) Nested sampling for general bayesian computation. Bayesian Analysis 1(4):833–859

[45] Skjervheim JA, Evensen G, Aanonsen SI, Ruud BO, Johansen TA (2007) Incorporating 4D seismic data in reservoir simulation models using ensemble Kalman filter. SPE Journal 12(3):282–292, DOI 10.2118/95789-PA

[46] Strebelle S (2002) Conditional simulation of complex geological structures using multiple-point statistics. Mathematical Geology 34(1):1–22

[47] Tavakoli R, Pencheva G, Wheeler MF, Ganis B (2012) A parallel ensemble-based framework for reservoir history matching and uncertainty characterization. Computational Geosciences 17(1):83–97, DOI 10.1007/s10596-012-9315-1

[48] Tavakoli R, Srinivasan S, Wheeler MF (2014) Rapid updating of utochastic models using an ensemble filter approach. SPE Journal 19(3):500–513, DOI http://dx.doi.org/10.2118/163673-PA

[49] Zafari M, Reynolds AC (2007) Assessing the uncertainty in reservoir description and performance predictions with the ensemble Kalman filter. SPE Journal 12(3):382–391, SPE 95750-PA

[50] Zhao Y, Reynolds AC, Li G (2008) Generating facies maps by assimilating production data and seismic data with the ensemble Kalman filter(SPE-113990). In: 2008 SPE Improved Oil Recovery Symposium

[51] Zhou H, Gomez-Hernandez J, Franssen HJH, Li L (2011) An approach to handling non-gaussianity of parameters and state variables in ensemble kalman filtering. Advances in Water Resources 34:844–864